Experimental and numerical investigation of specific behaviour of fluoride ions during filtration of pure salt water solutions with titania membrane

Patrick Dutournié, Liva Dzene, Arnaud Ponche, T. Jean Daou, Sébastien Déon

Experimental and numerical investigation of specific behaviour of fluoride ions during filtration of pure salt water solutions with titania membrane

Patrick Dutournié[1*], *Liva Dzene*[1], *Arnaud Ponche*[1], *T. Jean Daou*[1], *Sébastien Déon*[2]

1- Institut de Science des Matériaux de Mulhouse (IS2M-UMR CNRS 7361), Université de Haute-Alsace, Université de Strasbourg, 15 Rue Jean Starcky, BP 2488, 68057 Mulhouse cedex, France, patrick.dutournie@uha.fr , liva.dzene@uha.fr , arnaud.ponche@uha.fr , jean.daou@uha.fr

2- Institut UTINAM (UMR CNRS 6213), Université de Bourgogne-Franche-Comté, 16 route de Gray, 25030 Besançon cedex, France, sebastien.deon@univ-fcomte.fr

Corresponding author: Patrick Dutournié, patrick.dutournie@uha.fr

Abstract

This work addresses the specific interactions between titania membrane and fluoride anions during ultrafiltration operation. In general, the salt transmission increases with salt concentration when pure salt-water solutions are ultrafiltrated, except for fluoride-based salts observed in our study, for which transmission decreased at low concentrations. This phenomenon was only observed with titanium dioxide membrane. A numerical tool based on a physical description of ionic mass transfer in porous material (generalized Nernst-Planck approach) was used to explore the modification-induced changes due to fluoride anions.

Numerical investigations showed a modification of the electric charge of the membrane surface in the pore at low fluoride concentrations. This phenomenon screened the electric effect in a completely reversible way, and then enhanced the ion mass transfer through the porous membrane. These modifications can be explained by the substitution of oxygen atom (providing the surface electric charge) with a fluoride ion which was screening the electric charge and facilitated the ion transfer.

Keywords

Titanium dioxide; ultrafiltration membrane; electric charge screening; ion transport modelling; interaction titanium-fluoride

1. Introduction

Separation processes using membrane technologies are widely used for industrial applications to lower the cost and to increase the effectiveness of the operations [1]. Indeed, these separation technologies are energy efficient, easy to control and do not require additional chemicals compared to other separation methods [2]. Nanofiltration and ultrafiltration are used in industry for various applications (separation, concentration, rectification, etc) of small solutes in low-viscosity solutions. For example, these technologies are widely used for waste water treatment [3-5], for separation or concentration in food industry [6], and for the recovery of a lead compound in pharmaceutical industry [7]. The choice of the membrane (ceramic, polymeric …) [8,9] and the driving process (pressure / concentration / electric) [10] depends on the intended application and the operating conditions (temperature, pH, organic solvents, etc.). Mineral membranes have many advantages: they can operate in harsh conditions [11], can be easily cleaned [12] and, considering their chemical composition, they are not very suitable for bacterial growth [13]. Nevertheless, in practice, these membranes are less effective and more expensive than polymeric membranes [14]. Thus, they are often used only for specific industrial applications requiring distinctive features [15]. Currently, the most used ceramic membranes on the market are titanium dioxide, zirconia and alumina membranes. They are made from a mineral core on which a thin layer (active layer) of metal oxide is deposited. These membranes are tubular, ensuring good mechanical performances. Titanium dioxide membranes are often used because they offer additional interesting properties (photo-catalytic, antifouling, etc.) [16,17].

The membrane performances depend on the operating conditions (T, pH, pressure, salt concentration, etc.) and on the interactions between the surface and ions in solution. Indeed, these interactions are various (e.g., van der Waals forces, adsorption, hydrogen bonding, hydrophobic repulsion) and are responsible of modifying the apparent electric surface charge

[18] and the dielectric effects in the pore [19]. Several studies dealing with filtration tests of pure salt-water solutions consider only two exclusion mechanisms (steric and electric) [20,21]. However, few studies had focused also on dielectric effects in the pore. These effects can have various causes: the difference of dielectric property between the solution and the pore wall, the polarity of water, the presence of surface charges, dipoles and hydrated ions. [22]. These effects should be taken into account to study membrane performances, especially for a nanoporous active layer [23].

It is challenging (if not impossible) to estimate the contribution of each mechanism in a nanopore experimentally. Therefore, numerical investigations using a knowledge-based model can then be considered as an effective way to understand and to study the global influence of these phenomena on the operating performance of a membrane. Such modelling approach requires a physical description of all exclusion contributions reflecting reality as closely as possible. Steric effects can be easily conceptualized by assuming the solvent and solutes transport through the pores of well-defined size. From an experimental point of view, the magnitude of this exclusion phenomena can be approached by filtrating uncharged solutes [24]. For the electric and dielectric exclusions, there is no possibility to estimate or well-describe their real influences. Some authors have developed experimental indirect techniques for their estimations, as for example, zetametry, streaming induced potential or electrochemical impedance spectroscopy [25-27]. Likewise, different more or less theoretical models were implemented in the mass transfer modelling [28,29]. Unfortunately, these approaches (experimental and numerical) lead to imperfect descriptions of these two exclusion phenomena. The current trend is to take into account these contributions via a global description (i.e., effective surface charge and a decrease of apparent permittivity in the pore, results of several effects) [30,31].

The main objective of this work is to investigate the specific behavior of fluoride ions

94 throughout filtration with a titanium dioxide ultrafiltration membrane at low cut off. For this
95 purpose, separation performances of pure salt-water solutions at different salt concentrations
96 were experimentally and numerically investigated. The results are interpreted by using the
97 numerical modeling in terms of both electric and dielectric effects.
98

99 **2. Materials and methods**

100 Tangential filtration tests were performed with a laboratory pilot plant provided by
101 Techniques Industrielles Appliquées (Bollène, France) detailed in previous study [32]. The
102 membrane used in this work (TiO_2-1) was a commercial titanium dioxide membrane (1 kDa)
103 provided by TAMI Industries (Nyons, France). Three others membranes were used to validate
104 the results, a titania membrane from the same manufacturer, called TiO_2-2 and two home-
105 made zeolite membranes (Na-Mordenite and bi-layer MFI zeolite), called MOR and MFI.
106 Both membranes were obtained from zeolite synthesis on macroporous tubular support
107 (alumina). The membrane preparations are detailed in our previous papers for Mordenite [33]
108 and for bilayer MFI [34].

109 The membrane technical data are: 7 mm inner diameter and 25 cm length. The feed solution is
110 in a tank (5 L), and the fluid flow is provided by a volumetric pump at 700 L/h (Reynolds
111 number ≈ 35,000). The concentration polarization effects may be neglected, because the fluid
112 flow is mainly turbulent. The temperature is maintained at 25°C by a cooling unit. The
113 transmembrane pressure is controlled by adjusting a manual valve from ΔP = 4 to 12 bar.
114 Feed and retentate solutions are recycled in the feed tank during filtration in order to operate
115 at constant concentration. Retentate and permeate are sampled for analysis at each operating
116 pressure.

The membrane was previously conditioned by filtrating pure water (demineralized water, conductivity < 0.1 µS/cm). Between each experimental filtration, the pilot was flushed with pure water until a residual conductivity inferior to 1 µS/cm was obtained, and a filtration of pure water was carried out to estimate the hydraulic performances of the membrane. The membrane hydraulic permeability (L_p) was deduced from the slope of the linear curve (permeation flux (Jv) versus transmembrane pressure - Equation 1). µ is the dynamic viscosity of pure water.

$$J_v = L_p \frac{\Delta P}{\mu} \quad (1)$$

Filtration of vitamin B12 (Alfa Aesar, purity 98%, 9.10^{-4} mol.m^{-3}) – water solution was performed to investigate steric effects via the estimation of a mean pore radius of the membrane. The samples were analyzed by using an UV-visible spectrophotometer (Lambda 35, Perkin Elmer Instrument, Waltham, MA, USA) at 362 nm. Filtration of saline aqueous solutions were done with NaF and NaCl (Sigma-Aldrich, St. Quentin Fallavier, France, purity > 99%) at different concentrations (from 0.5 to 100 mol m^{-3}). Retentate and permeate (C_r and C_p, respectively) samples were analyzed by conductimetry (conductimeter PC 5000 L Phenomenal, VWR, Radnor, US). The permeation flux (Jv) was estimated by sample weighting.

The observed rejection rate R was deduced from the following equation:

$$R = 1 - \frac{C_p}{C_r} \quad (2)$$

3. Numerical modelling

Abundant works were devoted to numerical mass transfer in porous media and especially in membrane filtration. In nanofiltration or ultrafiltration at low cut-off, three modelling

139 approaches are commonly used to describe the transport of ionic and uncharged solutes in the
140 porous medium:

141 - The Kedem and Katchalsky equations [35], which derive from the thermodynamic
142 of irreversible processes. This approach can be used at different levels of
143 complexity, but is often used in its simpler form reducing the physical and
144 phenomenological descriptions.
145 - The Maxwell-Stefan equations [36], which relate the mass flow of each
146 components to the effects of driving forces. This rigorous approach requires the
147 estimation of different properties and parameters which are not easily accessible or
148 measurable.
149 - The Nernst-Planck equations [37] also derived from the thermodynamic of
150 irreversible processes and of systems far off the balance. Flux-force relations are
151 simplified by considering simplified equations with respect to the physical
152 description [38]. Commonly, the mass transfer is assumed to be one-dimensional
153 through uniform and cylindrical pores. The mass transfer in the pores is due to
154 three effects: diffusion (gradient of activity), electro-migration (electrical potential)
155 and convection [39].

156 The flux of an ionic solute (J_i) can be written in steady state according to these previous
157 assumptions as follow:

158 $$J_i = -K_{iD} D_i \frac{dC_i}{dx} - K_{iD} D_i c_i \frac{dln\gamma_i}{dx} - K_{iD} D_i z_i c_i \frac{F}{RT} \frac{d\Psi}{dx} + K_{ic} c_i V = V C_{ip} \quad (3)$$

159 The boundary conditions at both sides of the membrane active layer (x = 0, x = L) is an
160 equality of generalized chemical potentials of each solute at the interfaces between bulk and

pore solutions [40]. This equilibrium is often described by the product of three contributions: a steric, an electric and a dielectric one (equation 4).

For x = 0 or L $$\frac{c_i(x)}{C_i} = \phi_i \frac{\gamma_{is}}{\gamma_{ip}} \exp(-\Delta W_i) \exp\left(-\frac{z_i F}{RT} \Delta\Psi_D\right) \quad (4)$$

$\Delta\psi_D$ is the Donnan potential (difference in electrical potential at both sides of the interface free solution/solution in the pore). The steric effects are taken into account through $\phi_i = \left(1 - \frac{r_{is}}{r_p}\right)^2$ the steric partitioning coefficient which depends on the ratio of pore (r_p) and solute radii (r_{is}) [41].

ΔW_i estimates the dielectric effects. This term represents a sum of different interactions between solutes, solvent and membrane. For example, the confinement of water molecules in the pore, the difference of dielectric constant between the solvent and the pore surface, the ions hydration, etc.

Faced with the complexity of interacting phenomena, this contribution is often estimated (Born Model) via a modification of the apparent dielectric permeability (ε_p) of the solution in the pore. [42].

$$\Delta W_i = \frac{(z_i e)^2}{8\pi\varepsilon_0 r_{is} k_B T}\left(\frac{1}{\varepsilon_p} - \frac{1}{\varepsilon_b}\right) \quad (5)$$

Equations 3, 4 and 5 are solved for each ion by taking into account the electroneutrality in the feed solution and in the pore as follows:

$$\sum_{i=1}^{n} z_i C_i = 0 \quad \text{and for } 0 \le x \le L \sum_{i=1}^{n} z_i c_i(x) + X_d = 0 \quad (6)$$

Where X_d is the volumetric membrane charge density in the pore.

The permeation flux is calculated from Equation 7. $\Delta\pi$ is the osmotic pressure due to the difference of salt concentrations on both sides of the membrane.

$$J_v = \frac{L_p}{\mu}(\Delta P - \Delta\pi) \tag{7}$$

In the case of the filtration of a neutral solute, this set of equations is considerably simplified by neglecting electro-migration described in equation 3, electric and dielectric effects in the partitioning equations, the membrane charge and the osmotic pressure. Solving equation 3 and the appropriate boundary conditions (equation 4 at x = 0 and x = L) leads to an algebraic solution (equation 8) linking the observed rejection R to a mean pore radius r_p.

$$R = 1 - \frac{\phi K_c}{1 - (1 - \phi K_c)\exp\left(-\frac{K_c r_p^{\,2} \Delta P}{8\mu K_d D}\right)} \tag{8}$$

The pore is discretized according to the pore length (x), and concentration of each ion in the pore is obtained by consecutive integration. The set of equations is solved iteratively owing to the presence of the permeate concentration in the differential mass transfer equation (3). The program is written in Fortran 90.

Solving this model requires the estimation of 4 parameters (mean pore radius, hydraulic permeability, membrane charge and apparent dielectric constant in the pore). The hydraulic permeability was estimated from pure water filtration tests using equation 1. The mean pore radius was assessed via the filtration of a neutral molecule (vitamin B12) and the use of equation 8 (numerical approximation by minimizing quadratic error between experimental and calculated rejections). The membrane electric charge and apparent dielectric constant in the pore were estimated by fitting experimental results with the model.

So, the salt concentration of the solution C, the hydraulic permeability Lp and the mean pore radius rp are the input parameters. The calculation is done for five applied pressures ranging

from 4 to 12 bar. The simulation results are the permeate concentration and the permeate flow rate for each applied pressure. The calculation is repeated up to the experimental and numerical results are in good agreements by adjusting the membrane electric charge and the dielectric constant.

4. Results and Discussion

4.1. Experimental results

Before using the model, the estimation of both, hydraulic permeability and mean pore radius, are required. For this, a filtration test of pure water was performed by increasing and decreasing the applied pressure. The results are shown in figure 1. The water flux is a linear function of the applied pressure. The slope of the curve is the membrane hydraulic permeability divided by the dynamic viscosity ($L_p = 5.1\ 10^{-14}\ m^3 m^{-2}_{memb}$).

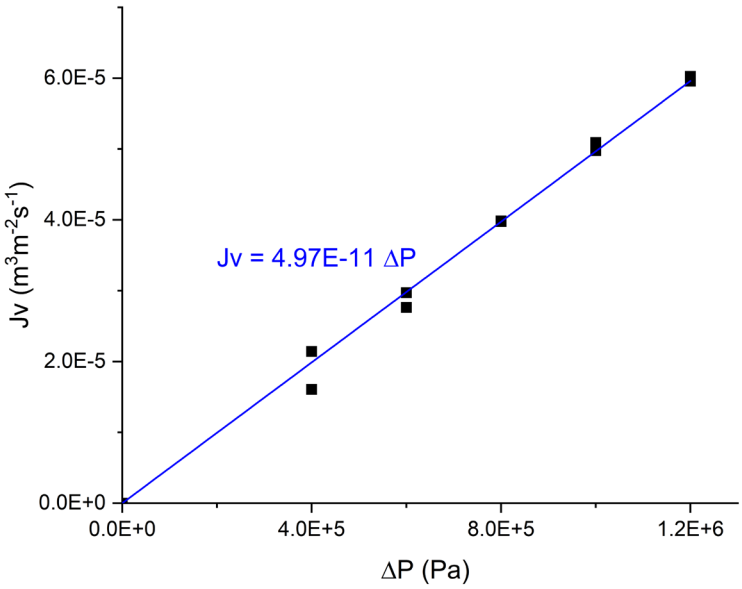

Figure 1: filtration of pure water (flow rate vs. transmembrane pressure).

Two experimental filtrations of vitamin B12-water solution were performed in order to estimate the steric effects. Figure 2 shows the experimental rejection rate of vitamin B12 as a function of the permeate flux. The mean pore radius was adjusted in equation 8 (red curve) to minimize quadratic difference between experimental and calculated rejection rates. The obtained mean pore radius was $r_p = 1.3$ nm.

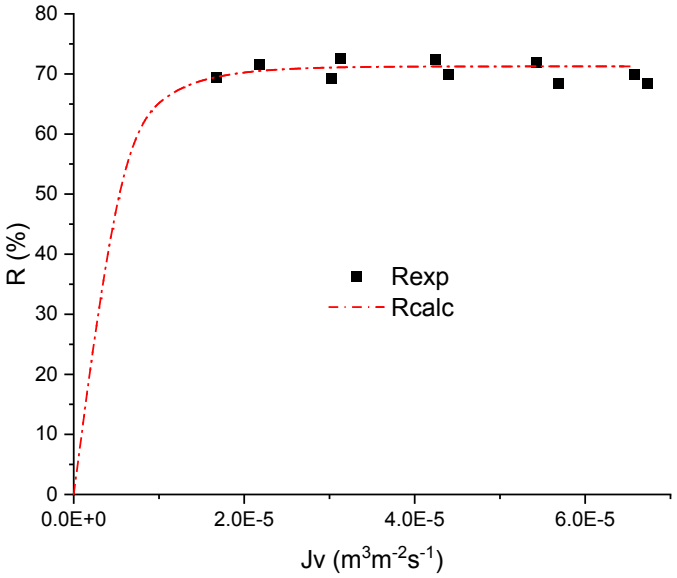

222

223 Figure 2: Experimental and calculated rejection rate of vitamin B12.

224 Successive filtration tests of pure salt – water solutions were performed for different salt
225 concentrations (from 0.5 to 100 mol.m^{-3}). Some tests were repeated (not in chronological
226 order) to exclude a gradual modification of the membrane properties (selectivity and / or
227 hydraulic).

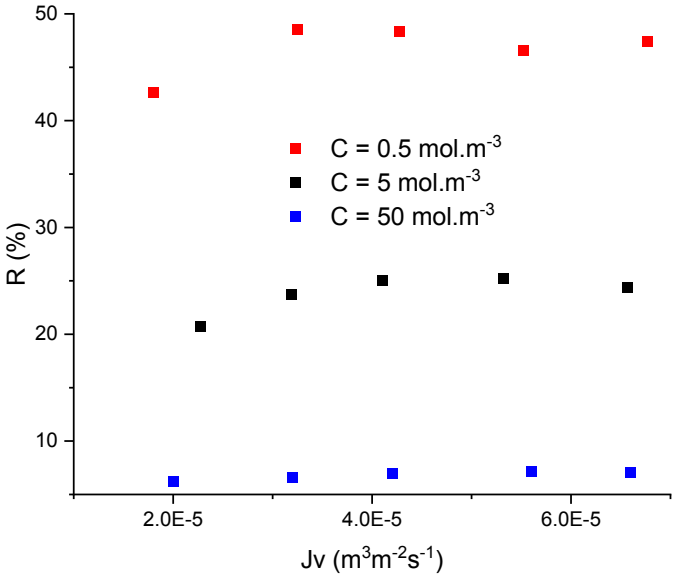

228

229 Figure 3: Experimental rejection rates of NaCl-water solutions (0.5 / 5 / 50 mol.m^{-3}).

230 Figure 3 shows the observed rejection rates obtained for filtration of sodium chloride–water
231 solutions at different salt concentrations. The rejection rate increased up to a maximal value of
232 about 8 bar for the transmembrane pressure. This maximum is plotted for all the filtration
233 experiments in a rejection rate / salt concentration diagram (figure 4).

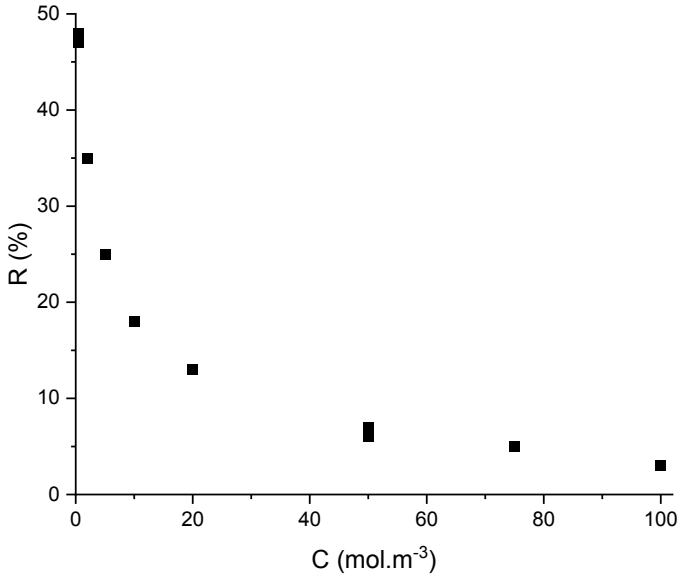

234

235 Figure 4: maximal rejection rates of NaCl-water solutions vs. salt concentration.

236 As it was expected, the maximum rejection rate decreased with the salt concentration
237 increasing. Indeed, this observation [43-45] was explained by the screening of the surface
238 electrical charge in the pore ($\frac{X_d}{C}$ decreases when C increases). The same experiments carried
239 out with other salts (NaI and Na_2SO_4) showed the same behaviour (figure S1 in
240 supplementary materials). Nevertheless, experiments with sodium fluoride show a peculiar
241 behaviour, especially at low salt concentrations. Figure 5 shows the maximum rejection rates
242 obtained with NaF-water solutions.

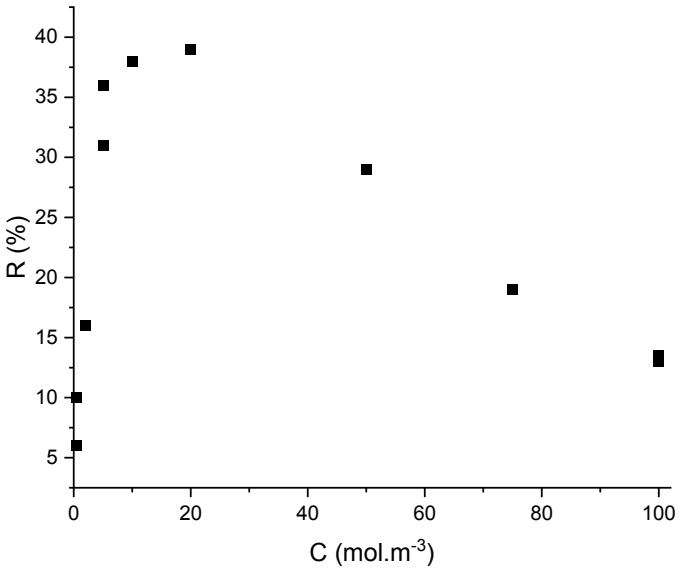

Figure 5: maximal rejection rates of NaF-water solutions vs. salt concentration.

The results showed a phenomenon occurring at low salt concentration facilitating the sodium fluoride transmission. When the salt concentration increased, a competition between this phenomenon and the screening of electrical charge was observed between 5 and 20 $mol.m^{-3}$. Beyond this concentration, the membrane separated in a normal way this saline solution. The observed phenomenon is fully reversible because some experiments at low concentration were additionally performed at the end of the series, and the results were similar.

Additional experiments performed with three different ceramic membranes showed the same results (figure 6) for both titanium dioxide membranes (TiO_2-1 and 2) and different results for both zeolite membranes. Indeed, the results obtained with MOR and MFI membranes showed

the same tendencies observed with the filtration of other salts, indicating that the peculiar behaviour observed in the case of titania membranes was due to a specific interaction between fluoride ions and titanium atoms.

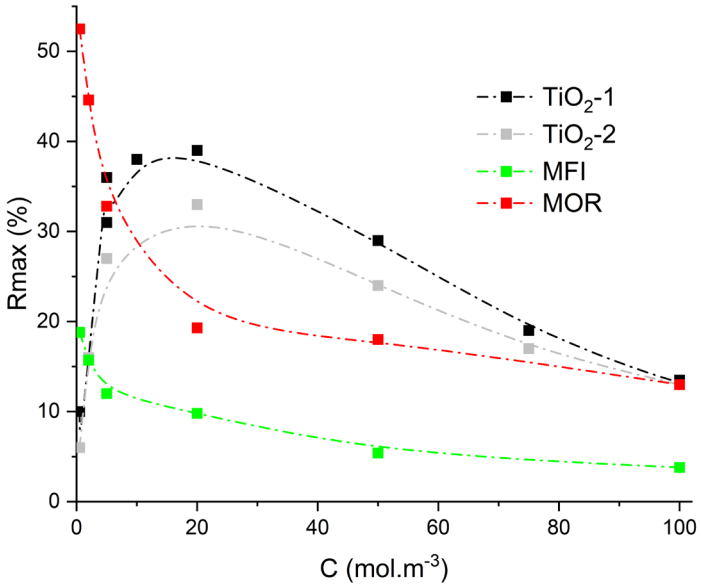

Figure 6: maximal rejection rates of NaF-water solutions obtained with different ceramic membranes.

4.2. Numerical investigation

A numerical approximation of rejection rate curves (R = f(Jv)) was performed by using the model previously described. The hydraulic permeability and the mean pore radius estimated from experimental results were used for the simulation, and the fitting was carried out by adjusting electric membrane charge (X_d) and dielectric permeability of the solution in the pore (ε_p). The numerical approximation lead to an infinity of couples (X_d, ε_p) that allowed a well-fitting of the rejection curves. This set of couples formed a curve. Figure 7 shows the best-fitted parameters' curves for each test performed in an electric charge / dielectric permittivity

271 diagram. Only negative values of the membrane electric charge were considered based on
272 previous zetametry investigations [46].

273

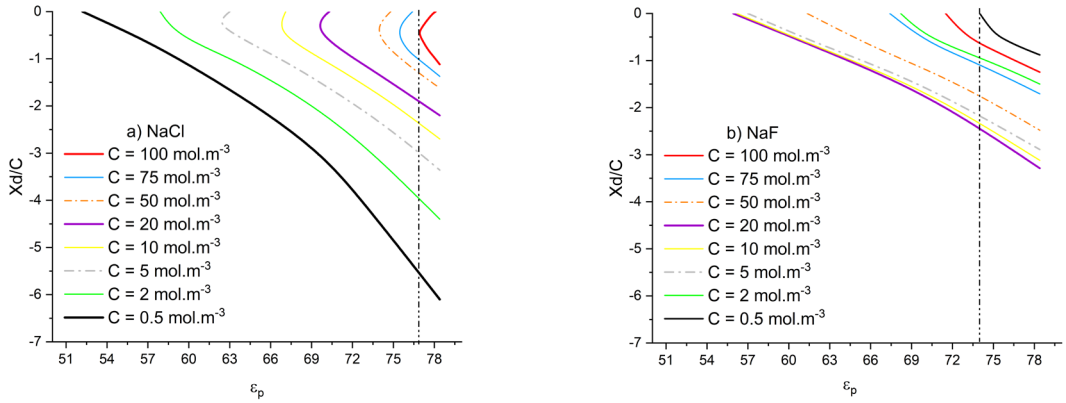

274

275 Figure 7: best-fitted (X_d, ε_p) for a) NaCl-water solutions and b) NaF-water solutions.

276 If the shapes of the curves were similar, the results obtained for NaF-solutions differed in
277 ascending order. Indeed, for NaCl-water solutions, the increase of salt concentration was
278 reflected in a diminution of both, electrical charge and dielectric exclusion. For NaF-water
279 solutions, dielectric exclusion and membrane electrical charge first increased to reach a
280 maximum (in the range C0 = 5-20 mol.m^{-3}) and then decreased. Theoretically, the dielectric
281 exclusion is the consequence of confinement, i.e., the difference of dielectric permittivity
282 between the solvent and the pore wall and the presence of ions in the pore. The more ions in
283 the pore, the more the dielectric exclusion is important. So, it can be assumed that the
284 maximal dielectric exclusion can be reached for high concentrations of salt. With this
285 hypothesis, the range (X_d, ε_p) could be reduced for each filtration test. Figure 8 shows the
286 range of surface membrane charge for each salt concentration.

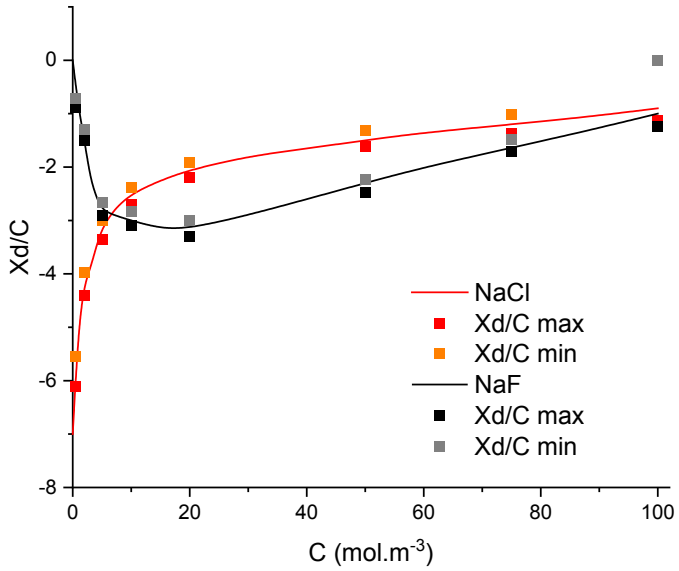

Figure 8: membrane electric charge for different salt concentrations (red = NaCl, black = NaF).

As expected, for NaCl-water solutions, the electric charge of the membrane was gradually screened by the salt concentration, reducing the electric exclusion. This finding was the same for different salts in solution, except sodium fluoride (only with titania membrane). For sodium fluoride – water solutions, it seems that there were two phenomena that drove the salt transmission in opposite directions. At high salt concentration, the behaviour was the same as NaCl (screening of electric charge in the pore). At low concentration, salt transfer was favoured instead as if the membrane electric charge (specific for each material) was screened by ions in the pore (reversible phenomenon).

The surface chemistry of titanium dioxide was often studied for photocatalytic applications. Several teams [47, 48] have studied F-doped TiO_2. They explained the increase of the catalytic properties by the creation of oxygen gaps and consequently an increase of surface acidity. Indeed, the surface charge (negative) is mainly due to oxygen. The substitution of O^{2-}

ions by F^- requires that $TiO_{2-x}(O^-)_x$ becomes $(TiO_{2-x})^+$-$(F^-)_x$ for maintaining the electro neutrality [49,50]. In this case, the interaction between fluoride ions and titania surface (figure 9) is due to electrostatic forces.

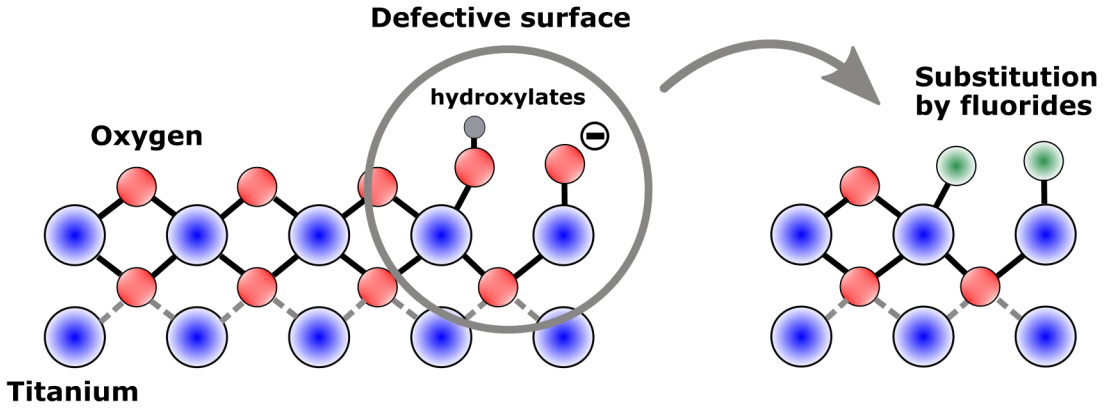

Figure 9: scheme of surface interaction.

This explanation agrees with all our observations, namely, the negative surface charge and a comparatively weak attraction explaining the reversibility and an increase of surface acidity. This phenomenon thus provides a less repulsive surface for fluoride anion and consequently an increase of salt transmission at low concentrations. Indeed, oxygen has an electric charge directed towards the fluid, while the fluoride charge is directed towards the surface attracted by the charge of the titanium atom.

5. Conclusion

Filtration of fluoride ions with a titanium dioxide membrane showed a specific behaviour different from the other salts. Indeed, at low salt concentrations, fluoride ions were mainly transmitted while chloride, iodide and other ions were predominantly rejected. The numerical study of these filtration tests indicated that the electric charge in the pore (scaled by the salt concentration) was very low at low concentrations in contrast with sodium chloride (the ratio between the electric charge in the pore and the salt concentration is maximal at low

concentrations). This can be explained by a specific and reversible interaction between titanium and fluoride ions modifying the surface chemistry in the pores. A partial substitution of O^{2-} ions by F^- imparted a quasi-neutral electric charge in the pore facilitating the transfer of ions.

Glossary

c_i	Concentration of ion i in the pore (mol m^{-3})
C_{ip}	Permeate concentration of ion i (mol m^{-3})
C_{ir}	Bulk concentration of ion i (mol m^{-3})
$C0$	Average salt concentration in the feed solution (mol m^{-3})
D_i	Diffusion coefficient of ion i at infinite dilution (m^2 s^{-1})
e	Electronic charge (1.602 10^{-19} C)
F	Faraday constant (96487 C mol^{-1})
J_i	Flux of ion i (mol m^{-2} s^{-1})
J_v	Permeation flux (m^3 m^{-2} s^{-1})
J_w	Permeation flux of pure water (m^3 m^{-2} s^{-1})
k_B	Boltzmann constant (1,381 10^{-23} m^2 kg s^{-2} K^{-1})
K_{ic}	Hindrance factor for convection relative to ion i(dimensionless)
K_{id}	Hindrance factor for diffusion of ion i (dimensionless)
L_p	Hydraulic permeability ($m^3 m_{memb}^{-2}$)
R	Gas constant (8.314 J mol^{-1} K^{-1})
r_{is}	Stokes radius of ion i (m)
R_i	Observed rejection of ion i (dimensionless)
r_p	Average pore radius (m)
T	Temperature (K)
V	Solvent velocity in the pore (m.s^{-1})
x	Axial position within the pore (m)
X_d	Apparent electric charge density in the membrane pore (eq m^{-3})
z_i	Valence of ion i (dimensionless)

- Greek letters

γ_{ip}	Activity coefficient of ion i in the pore (dimensionless)
γ_{is}	Activity coefficient of ion i in the feed solution at the pore inlet (dimensionless)
ΔP	Transmembrane pressure (Pa)
ΔW_i	Dielectric exclusion energy (J)
$\Delta \psi_D$	Donnan potential (V)
$\Delta \pi$	Osmotic pressure difference (Pa)
ε_0	Permittivity of free space (8.85419 10^{-12} F.m^{-1})
ε_b	Bulk dielectric constant (dimensionless) = 78.4
ε_p	Pore dielectric constant (dimensionless)

μ	Dynamic viscosity (Pa s)
ϕ_i	Steric partition coefficient (dimensionless)
ψ	Electrical potential within the pore (V)

Funding

This research did not receive any specific grant from funding agencies in the public, commercial, or not-for-profit sectors.

References

[1] J. P. Chen, H. Mou, L. K. Wang, T. Matsuura, Y. Wei, Membrane Separation: Basics and applications in L.K. Wang, J.P. Chen, Y.T. Hung, N.K. Shammas (Eds.), Membrane and desalination technologies, Springer, New York, 2011, pp 271-332.

[2] R.W. Baker, Membrane technology and applications., John Wiley & Sons, Chichester, 2004.

[3] B. Van der Bruggen, M. Mänttäri, M. Nyström, Drawbacks of applying nanofiltration and how to avoid them: A review, Sep. Purif. Technol., 63 (2008) 251-263.

[4] G. Pearce, Introduction to membranes: Filtration for water and wastewater treatment, Filtr. Sep., 44 (2007) 24-27.

[5] P. Zhang, J.L. Gong, G.M. Zeng, C.H. Deng, H.C. Yang, H.Y. Liu, S.Y. Huan, Cross-linking to prepare composite graphene oxide-framework membranes with high-flux for dyes and heavy metal ions removal, Chem. Eng. J., 322 (2017) 657-666.

[6] D. Knorr, A. Froehling, H. Jaeger, K. Reineke, O. Schlueter, K. Schoessler, Emerging Technologies in Food Processing, Annu. Food. Sci. Technol., 2 (2011) 203-235.

[7] A.K. Pabby, S.S.H. Rizvi, A.M.S. Requena, Handbook of Membrane Separations: Chemical, Pharmaceutical, Food, and Biotechnological Applications, CRC Press, Boca Raton, 2015.

[8] M. B. Asif, Z. Zhang, Ceramic membrane technology for water and wastewater treatment: A critical review of performance, full-scale applications, membrane fouling and prospects, Chem. Eng. J., 418 (2021) 129481.

[9] B. Hofs, J. Ogier, D. Vries, E. F. Beerendonk, E. R. Cornelissen, Comparison of ceramic and polymeric membrane permeability and fouling using surface water, Sep. Purif. Technol. 79 (2011) 365-374.

[10] T. Colinart, S. Didierjean, O. Lottin, G. Maranzana, C. Moyne, Transport in PFSA membranes, Journal of the electrochemical society 155 (2008) B244.

[11] K. Kimaru, H. Uchida, Intensive membrane cleaning for MBRs equipped with flat-sheet ceramic membranes: Controlling negative effects of chemical reagents used for membrane cleaning, Water Res. 150 (2019) 21-28.

[12] R. Xiong, G. Sun, K. Si, Q. Liu, K. Liu, Pressure drop prediction of ceramic membrane filtrers at high temperature, Powder technology, 364, 2020, 647-653.

[13] J. Xu, C.-Y. Chang, J. Hou, C. Gao, Comparison of approaches to minimize fouling of a UF ceramic membrane in filtration of seawater, Chem. Eng. J. 223 (2013) 722-728.

[14] K. Bin Bandar, M. D. Alsubei, S. A. Aljlil, N. Bin Darwish, N. Hilal, Membrane distillation process application using a novel ceramic membrane for brackish water desalination, Desalination 500 (2021) 114906.

[15] N. Rahimi, R.A. Pax, E.A. Gray, Review of functional titanium oxides. I: TiO_2 and its modifications. Prog. Solid State Chem. 44 (2016) 86-105.

[16] S. Mozia, K. Szymański, B. Michalkiewicz, B.Tryba, M. Toyoda, A.W. Morawski, A.W. Effect of process parameters on fouling and stability of MF/UF TiO_2 membranes in a photocatalytic membrane reactor. Sep. Purif. Technol. 142 (2015) 137-148.

[17] M. Hatat-Fraile, R. Liang, M.J. Arlos, R.X. He, P. Peng, M.R. Servos, Y.N. Zhou, Concurrent photocatalytic and filtration processes using doped TiO_2 coated quartz fiber membranes in a photocatalytic membrane reactor, Chem. Eng. J. 330 (2017) 531-540.

[18] A. Silva, F. Martín, J. Martínez, P. Malfeito, L. Prádanos, L. Palacio, A. Hernández, Electrical characterization of NF membranes. A modified model with charge variation along the pores, Chem. Eng. Sci. 66 (2011) 2898-2911.

[19] P. Dutournié, S. Déon, L. Limousy, Understanding the separation of anion mixtures by TiO_2 membranes: Numerical investigation and effect of alkaline treatment on physicochemical properties, Chem. Eng. J. 363, 2019, 365-373.

[20] Z. Wang, K. Xiao, X. M. Wang, Role of coexistence of negative and positive membrane surface charges in electrostatic effect for salt rejection by nanofiltration, Desalination 444 (2018) 75-83.

[21] P. Árki, C. Hecker, G. Tomandl, Y. Joseph, Streaming potential properties of ceramic nanofiltration membranes – Importance of surface charge on the ion rejection, Sep. Purif. Technol., 212 (2019) 660-669.

[22] F. E. Ahmed, R. Hashaikeh, A. Diabat, N. Hilal, Mathematical and optimization modelling in desalination: State-of-the-art and future direction, Desalination 469 (2019) 114092.

[23] A.E. Yaroshchuk, Dielectric exclusion of ions from membranes, Advances in colloid and interface science 85 (2000) 193-230.

[24] W.R. Bowen, J.S. Welfoot, P.M. Williams, Linearized transport model for nanofiltration: Development and assessment, AIChE J. 48 (2002) 760-773.

[25] A.A. Hussain, S.K. Nataraj, M.E.E. Abashar, I.S. Al-Mutaz, T.M. Aminabhavi, Prediction of physical properties of nanofiltration membranes using experiment and theoretical models, J. Membr. Sci. 310 (2008) 321-336.

[26] P. Árki, C. Hecker, G. Tomandl, Y. Joseph, Streaming potential properties of ceramic nanofiltration membranes – Importance of surface charge on the ion rejection, Sep. Purif. Technol. 212 (2019) 660-669.

[27] M. Montalvillo, V. Silva, L. Palacio, J.I. Calvo, F.J. Carmona, A. Hernández, P. Prádanos, Charge and dielectric characterization of nanofiltration membranes by impedance spectroscopy, J. Membr. Sci. 454 (2014) 163-173.

[28] V. Freger, S. Bason, Characterization of ion transport in thin films using electrochemical impedance spectroscopy: I. Principles and theory, J. Membr. Sci., 302 (2007) 1-9.

[29] P. Fievet, M. Sbaï, A. Szymczyck, A. Vidonne, Determining the ζ-potential of plane membranes from tangential streaming potential measurements: effect of the membrane body conductance, J. Membr. Sci. 226 (2003) 227-236.

[30] S. Déon, A. Escoda, P. Fievet, P. Dutournié, P. Bourseau, How to use a multi-ionic transport model to fully predict rejection of mineral salts by nanofiltration membranes, Chem. Eng. J. 189-190 (2012) 24-31.

[31] S. Déon, P. Dutournié, P. Fievet, L. Limousy, P. Bourseau, Concentration polarization phenomenon during the nanofiltration of multi-ionic solutions: Influence of the filtrated solution and operating conditions, Water Res. 47 (2013) 2260-2272.

[32] S.M. Miron, P. Dutournié, K. Thabet, A. Ponche, Filtration of protein based solutions with ceramic ultrafiltration membrane. Study of selectivity, adsorption and protein denaturation, Comptes rendus de Chimie 22 (2019) 198-205.

[33] P. Dutournié, L. Limousy, N. Zouaoui, H; Mahzoul, E. Chevereau, Facilitated transport of monovalent salt mixture through ultrafiltration Na-Mordenite membrane: Numerical investigations of electric and dielectric contributions, Desalination 280 (2011) 397-402.

[34] A. Said, L. Limousy, H. Nouali, L. Michelin, J. Halawani, J. Toufaily, T. Hamieh, P. Dutournié, T. J. Daou, Synthesis of mono- and bi-layer MZI seolite films on macroporous alumina tubular supports: Application to nanofiltration, Journal of Crystal Growth 428 (2015) 71-79.

[35] H. Al-Zoubi, N. Hilal, N.A. Darwish, A.W. Mohammad, Rejection and modelling of sulphate and potassium salts by nanofiltration membranes: neural network and Spiegler-Kedem model, Desalination 206 (2007) 42-60.

[36] T.R. Noordman, J.A. Wesselingh, Transport of large molecules through membranes with narrow pores. The Maxwell-Stefan description combined with hydrodynamic theory, J. Membr. Sci. 210 (2002) 227-243.

[37] W.R. Bowen, J.S. Welfoot, Modelling the performance of membrane nanofiltration-critical assessment and model development, Chem. Eng. Sci. 57 (2002) 1121-1137.

[38] S. Déon, P. Dutournié, L. Limousy, P. Bourseau, The two-dimensional pore and polarization transport model to describe mixtures separation by nanofiltration: Model validation, AIChE J. 57 (2011) 985-995.

[39] A. Szymczyck, C. Labbez, P. Fievet, A. Vidonne, A. Foissy, J. Pagetti, Contribution of convection, diffusion and migration to electrolyte transport through nanofiltration membranes, Advances in Colloid and Interface Science 103 (2003) 77-94.

[40] T. Gimmi, P. Alt-Epping, Simulating Donnan equilibria based on the Nernst-Planck equation, Geochemica et cosmochimica Acta 232 (2018) 1-13.

[41] W. R. Bowen, A. W. Mohammad, N. Hilal, Characterisation of nanofiltration membranes for predictive purposes – Use of salts, uncharges solutes and atomic force microscopy, J. membr. Sci. 126 (1997) 91-105.

[42] S. Déon, P. Dutournié, L. Limousy, P. Bourseau, Transport of salt mixtures through nanofiltration membranes: Numerical identification of electric and dielectric contributions, Sep. Purif. Technol. 69 (2009) 225-233.

[43] J.S. D'Arrigo, Screening of membrane surface charges by divalent cations: an atomic representation, American Journal of Physiology-Cell Physiology, 235 (1978) C109.

[44] H. L. Petrache, T. Zemb, L. Belloni, V.A. Parsegian, Salt screening and specific ion adsorption determine neutral-lipid membrane interactions, PNAS 103 (2006) 7982-7987.

[45] S. Li, S.G.J. Heijman, J.Q.J.C. Verberk, P. Le Clech, J. Lu, A.J.B. Kemperman, G.L.

Amy, J.C. van Dijk, Fouling control mechanisms of demineralized water backwash: Reduction of charge screening and calcium bridging effects, Water Res. 45 (2011) 6289-6300.

[46] P. Dutournié, L. Limousy, J. Anquetil, S. Déon, Modification of the selectivity properties of tubular ceramic membranes after alkaline treatment, Membranes 7 65 (2017) 7040065.

[47] D. Li, H. Haneda, S. Hishita, N. Ohashi, Visible-Light-Driven N−F−Codoped TiO_2 Photocatalysts. 2. Optical Characterization, Photocatalysis, and Potential Application to Air Purification. Chem. Mater. 17 (2005) 2596-2602.

[48] J. Xu, Y. Ao, D. Fu, C. Yuan, Low-Temperature Preparation of F-Doped TiO2 Film and Its Photocatalytic Activity under Solar Light. Applied Surface Science 254 (2008) 3033-3038.

[49] N. El Houda Ghanni, Etude DFT de l'influence des ions fluorure sur les mécanismes de croissance des oxides nanoporeux par oxidation anodique, PhD thesis, 2018, https://tel.archives-ouvertes.fr/tel-01879538.

[50] C. Minero, G. Mariella, V. Maurino, E. Pelizzetti, Photocatalytic transformation of organic compounds in the presence of inorganic anions. 1. Hydroxyl-mediated and direct electron transfer reactions of phenol on a titanium dioxide – fluoride system, Langmuir 16 (2000) 2632-2641.

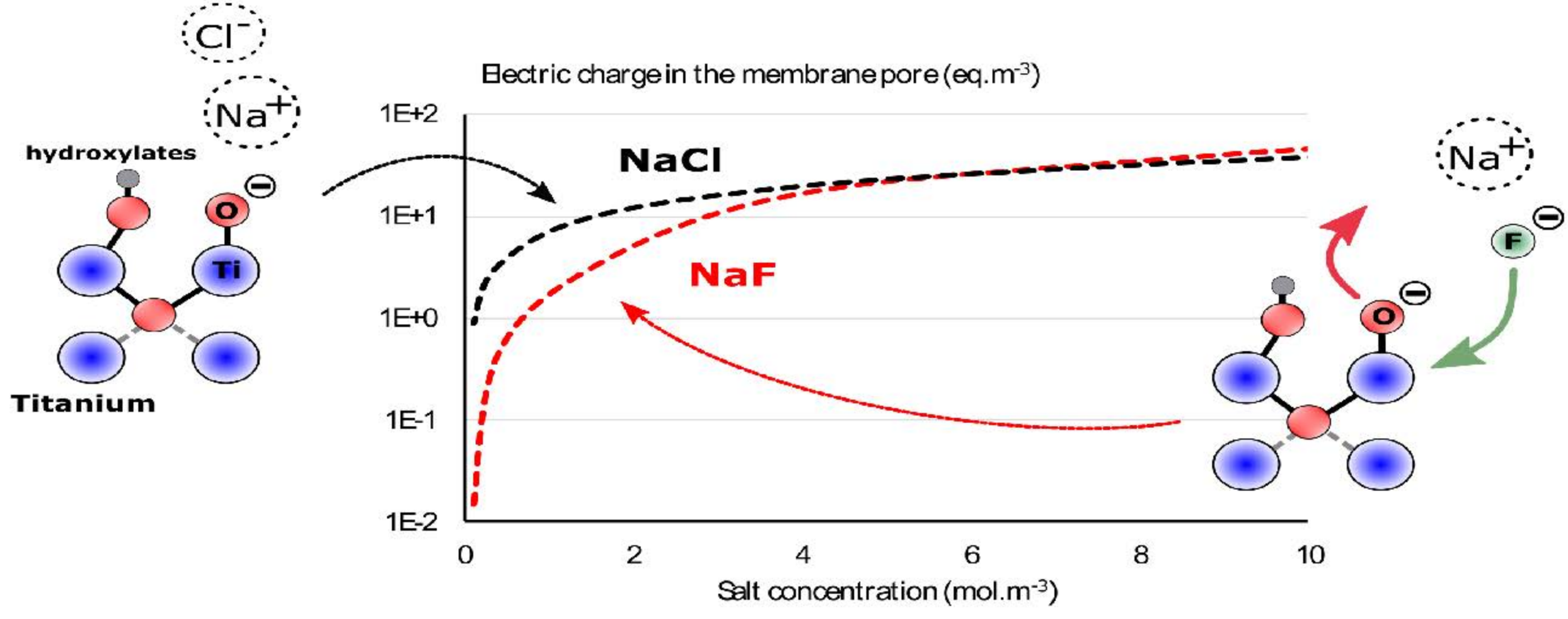
Cl⁻
Na⁺
hydroxylates
O
Ti
Titanium
Electric charge in the membrane pore (eq.m⁻³)
1E+2
1E+1
1E+0
1E-1
1E-2
NaCl
NaF
0
2
4
6
8
10
Salt concentration (mol.m⁻³)
Na⁺
F
O